

Variability of the North Pacific Current and its bifurcation

Patrick F. Cummins *, Howard J. Freeland

Institute of Ocean Sciences, Fisheries and Oceans Canada, P.O. Box 6000, Sidney, BC, Canada V8L 4B2

Available online 17 August 2007

Abstract

The North Pacific Current (NPC) bifurcates approaching the west coast of North America into a subpolar branch that forms the Alaska Current, and a subtropical branch that includes the California Current. The variability of this current system is discussed using numerical results from a wind-driven, reduced-gravity model. Indices of the strength of the subpolar and subtropical components of the NPC are examined based on output from multi-decadal simulations with the numerical model. This shows periods of both correlated and anti-correlated variability of the subpolar and subtropical gyres. A decomposition of the gyre transport time series indicates that the dominant mode of variability is a “breathing” mode in which the subpolar and subtropical gyres co-vary in response to fluctuations in the strength of the NPC. This finding is consistent with an analysis of dynamic height data of limited duration from the array of Argo drifting floats.

The variability of the NPC is also examined using sea surface height (SSH) data from satellite altimetry over the period 1993–2005. The leading mode of SSH over the northeast Pacific dominates the variability of the NPC and is shown to be associated with in-phase variations in the transport of the subtropical and subpolar gyres. A strong correlation is found between time-dependent fluctuations in SSH across the NPC and variations in the strength of the transport of the NPC in the model. This agreement provides evidence for variability of the NPC occurring in direct response to large-scale atmospheric forcing.

© 2007 Elsevier Ltd. All rights reserved.

Regional Index Terms: Pacific Ocean; Northeast Pacific; Gulf of Alaska

Keywords: Geostrophic transport; Wind driven circulation; Gyres; Sea surface height; Ekman pumping

1. Introduction

The North Pacific Current (NPC) is the broad, eastward directed, surface intensified flow that originates from the flow of the Kuroshio Extension in the central Pacific. Approaching the west coast of North America, the NPC bifurcates into northward and southward flowing branches that are associated with the subpolar and subtropical circulation gyres, respectively. The variability of the NPC and its bifurcation was considered by [Chelton and Davis \(1982\)](#) who examined 30 years of sea level anomalies from a network of coastal tide gauges. They found a dominant pattern of low frequency variability consisting of in-phase coastal sea level variations

* Corresponding author.

E-mail address: cumminsp@dfo-mpo.gc.ca (P.F. Cummins).

extending from Mexico to the Aleutian Islands. It was suggested that this mode is associated with anti-correlated variations in the intensity of the subpolar and subtropical branches of the NPC. In the following, this mode of variability is referred to as a “bifurcation mode”, characterized by a constant transport of the NPC and mutually compensating variations in the strength of its subpolar and subtropical components.

The variability of the NPC has been examined in two recent papers. [Douglass et al. \(2006\)](#) considered data from two XBT sections in the eastern Pacific over the period 1993–2002, as well as simulations with a data assimilating model. Their results showed evidence for the occurrence of anti-correlated variations in the transports of the Alaska and California Currents, in accordance with the hypothesis of [Chelton and Davis \(1982\)](#). However, the authors also note that the “dominant signal is found to be a long-term increase in the NPC, which results in a strengthening of the subtropical gyre”.

[Freeland \(2006\)](#) addressed the issue of the bifurcation using four years of hydrographic data from the Argo array of drifting floats in the northeast Pacific. Monthly maps of the absolute surface geostrophic circulation were constructed based on the method outlined in [Freeland and Cummins \(2005\)](#). Using these geostrophic circulation fields, a dividing streamline was identified and time series were formed of dynamic height differences across the subpolar and subtropical gyres, denoted $\Delta D_{SP}(t)$ and $\Delta D_{ST}(t)$, respectively. By definition, the dynamic height difference across the NPC is taken as $\Delta D_{NPC}(t) = \Delta D_{SP}(t) + \Delta D_{ST}(t)$. [Freeland \(2006\)](#) discussed the decomposition of these time series into two distinct modes of variability. The bifurcation mode discussed above was identified. In addition, evidence was found for a “breathing mode” that is characterized by in-phase variations in the subpolar and subtropical gyres. The results based on dynamic heights from Argo suggested that the preponderance of the variability was associated with the breathing mode, while the bifurcation mode accounted for a relatively small fraction of the variance.

The chief limitation of an analysis based on Argo observations is the relatively short duration of the available data. This may be an important consideration given the pronounced variability that is known to occur on inter-annual to decadal time-scales in the extratropical North Pacific (e.g., [Lagerloef, 1995](#); [Zhang et al., 1997](#)). In this paper, results from extended numerical simulations with a wind-driven, reduced-gravity, quasi-geostrophic model are considered. The numerical results are applied to examine the variability of the NPC and the partition of variance between the breathing and bifurcation modes. In addition, sea surface height (SSH) differences across the NPC based on satellite altimeter data are used to examine the variability over the period 1993–2005. These data are compared with the numerical simulations and with the available Argo data.

We have found that the method discussed by [Freeland \(2006\)](#) to examine the bifurcation has an implicit bias to assign excessive variance to the breathing mode. Accordingly, a new approach was adopted to decompose time series of gyre variability into breathing and bifurcation modes. This method is outlined in the [Appendix](#), which also includes a reanalysis of the time series of Argo dynamic heights. The results are nevertheless consistent with the conclusions of [Freeland \(2006\)](#) and show that the most of the variance in the Argo time series (65%) resides in the breathing mode.

In the following section, results from the reduced-gravity model are presented. In Section 3, the variability of the NPC based on T/P-Jason altimeter data are discussed and compared with Argo data and model results. Conclusions are drawn in Section 4.

2. Variability of the NPC in a reduced-gravity model

The statistical properties of the variability of the NPC are considered in long-term integrations with a linear, wind-driven, reduced-gravity, quasi-geostrophic model. Models of this type have been shown to have skill in representing SSH and upper-layer thickness variability over the northeast Pacific ([Lagerloef, 1995](#); [Qiu, 2002](#); [Cummins and Lagerloef, 2002, 2004](#); [Fu and Qiu, 2002](#); [Capotondi et al., 2005](#)). The numerical model has been discussed previously in [Cummins and Lagerloef \(2004\)](#). It solves a vorticity equation governing the evolution of the (positive upwards) interfacial displacement, h , on a spherical coordinate grid that extends over the extratropical North Pacific with a uniform horizontal resolution of 1/3 degree in latitude and longitude. The only modification to the model is the replacement of biharmonic lateral friction with Laplacian friction with a viscosity of $500 \text{ m}^2 \text{ s}^{-1}$. The model is forced with time-varying wind stress curl (Ekman pumping) for the period 1948–2005. These fields were derived from monthly mean wind stresses from the NCEP reanalysis ([Kalnay et al., 1996](#)).

The main governing parameters of the model are the linear drag coefficient with a damping time-scale given by λ^{-1} and the deformation radius given by $R(\theta) = \sqrt{g'H}/f$. The Coriolis parameter is $f(\theta)$ with θ the latitude. The reduced gravity is g' and H is the undisturbed depth of the upper layer. In the linear quasi-geostrophic model it is not necessary to specify g' and H independently. The parameter choice $g'H = 7.5 \text{ m}^2 \text{ s}^{-2}$ is adopted for the basic numerical experiment. This value was shown previously to lead to a reasonable fit to the longitudinally averaged long Rossby wave speeds, although it somewhat overestimates wave speeds at high latitudes (Cummins and Lagerloef, 2004). The sensitivity of the results to a reduced value ($g'H = 6 \text{ m}^2 \text{ s}^{-2}$) that provides a better fit at higher latitudes was explored. A uniform damping time-scale of $\lambda^{-1} = 3$ years was adopted for the basic experiment. In comparisons with altimeter data, Cummins and Lagerloef (2004) found that this value is close to optimal when the damping parameter is spatially uniform. The sensitivity of the results to this choice was also explored.

A geostrophic transport streamfunction, Ψ , may be defined in terms of the interfacial displacement, $\Psi = \Psi_B - H(g'h/f)$, such that the depth-integrated geostrophic flow is given by $(U, V) = \left(-\frac{\partial \Psi}{\partial y}, \frac{\partial \Psi}{\partial x}\right)$. Here, $\Psi_B = 0$ is the (constant) value of the streamfunction along the boundary. The streamfunction, Ψ , is decomposed into mean and fluctuating components, $\Psi = \langle \Psi \rangle + \Psi'$, where the angle brackets denote a time average and the primes denote deviations from the average. As the model is linear, the mean transport is driven by the mean wind stress curl forcing, while fluctuations in transport are due to the time varying component of the forcing.

Fig. 1 shows the mean transport streamfunction, $\langle \Psi \rangle$, for the upper ocean over the northeast Pacific in the basic numerical simulation. The flow pattern here is similar to that of the mean transport streamfunction of Douglass et al. (2006). The broad flow of the NPC and its bifurcation are evident with the flow splitting into subpolar and subtropical gyres. The northward flowing branch is identified with the Alaska Current. This current narrows near the head of the Gulf of Alaska, where it is renamed the Alaskan Stream, an intense western boundary current. A branch flows southward forming the broad subtropical gyre. As expected, away from the boundaries the response of the model conforms to Sverdrup balance and the time-averaged dividing streamline between the gyres, defined by the $\langle \Psi \rangle = 0$ contour, is aligned closely with the mean zero wind stress curl contour.

Time series of fluctuations in the transport of the subpolar and subtropical gyres were constructed from local spatial averages of Ψ' about the two reference locations, indicated in Fig. 1. Specifically, the transport

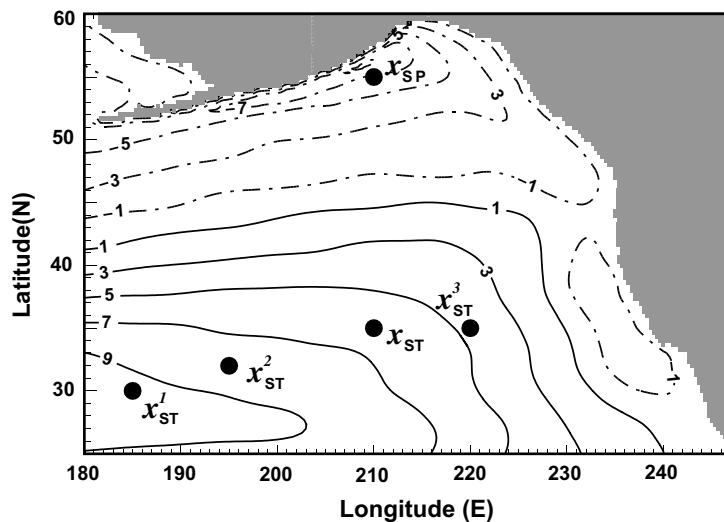


Fig. 1. Time-averaged transport streamfunction (in Sv) from the reduced-gravity model with a value for the damping parameter of $\lambda^{-1} = 3$ years. Flow is along the contours and in a clockwise (counterclockwise) sense for solid (dashed) contours. The locations x_{SP} and x_{ST} are used to gauge fluctuations in the transports of the subpolar and subtropical gyres, respectively. Also indicated are additional points in the subtropical gyre that are used to examine the sensitivity of the results to variations in the reference location.

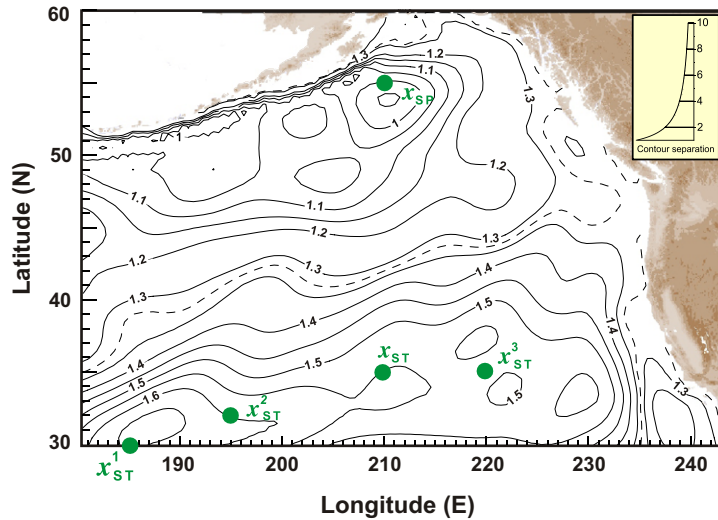


Fig. 2. Time-averaged dynamic height field (metres) from the Argo array of floats for the 4-year period, Oct. 2002–Sept. 2006. The dashed line indicates the streamline dividing the time-averaged subpolar and subtropical gyres. The reference locations shown in Fig. 1 are included.

fluctuations are defined as $T'_{SP}(t) = -\overline{\Psi}'(\mathbf{x}_{SP}, t)$ and $T'_{ST}(t) = \overline{\Psi}'(\mathbf{x}_{ST}, t)$, respectively. The overbars represent a 25-point spatial average over $4/3^\circ \times 4/3^\circ$ sectors centered at \mathbf{x}_{SP} (210°E 55° N) and \mathbf{x}_{ST} (210°E 35°N). These reference points were chosen to encompass approximately the upper layer transport into the subpolar and subtropical gyres, as indicated by the time-averaged field (Fig. 1). The same reference locations are also used below in Section 3 with respect to the altimeter data to examine SSH difference anomalies across the NPC.

Points \mathbf{x}_{SP} and \mathbf{x}_{ST} correspond approximately with locations that Freeland (2006) used to gauge the subpolar and subtropical gyre transports in the Argo data (e.g., see the lower right panel of his Fig. 3). These reference locations are superposed in Fig. 2 on the time-averaged surface geostrophic circulation over the northeast Pacific derived from 4 years of Argo observations over the period Oct. 2002–Sept. 2006¹. Point \mathbf{x}_{SP} is in proximity of the local minima in the mean dynamic height field near the head of the Gulf of Alaska. Point \mathbf{x}_{ST} , situated twenty degrees of latitudes to the south across the NPC, lies along a ridge in the mean dynamic height field. While local gradients are relatively weak, the location chosen for point \mathbf{x}_{ST} along this ridge of elevated dynamic height is somewhat arbitrary. Thus to examine the sensitivity of the results, a set of three other points along the ridge of elevated dynamic height were considered in the analysis. These are shown as points \mathbf{x}_{ST}^1 , \mathbf{x}_{ST}^2 and \mathbf{x}_{ST}^3 in Figs. 1 and 2. Relative to the mean circulation, these figures suggest that the magnitude of the subtropical gyre transport will depend on the choice of reference location with \mathbf{x}_{ST}^1 encompassing the greatest transport, and \mathbf{x}_{ST}^3 the least. It is worth emphasizing that the results presented below are not very sensitive to small variations in the position of the reference locations. They can be shifted by a few degrees in either direction without qualitative change to the results, provided \mathbf{x}_{SP} remains outside the frictional boundary layer. The results are also insensitive to the areal extent of the spatial averaging, which could be omitted.

The transport of the subtropical gyre includes the southward flowing California Current. As shown in Fig. 2, this current separates from the coast at about 40°N. Further south, the California Current is located well offshore and a recirculating, northward-flowing current (the Davidson Current) is found inshore, adjacent to the coast. This is also seen in the model transport streamfunction in Fig. 1. There may be no well-defined demarcation between the California Current and the interior flow of the subtropical gyre; climatological 0–1000 dB dynamic heights (Qiu, 2002) do not show a clear distinction between the two.

¹ Although Argo data from the northeast Pacific are available prior to this time, the sampling of the subtropical gyre was relatively sparse until the deployment of several floats between 30°N and 40°N in Sept. 2002.

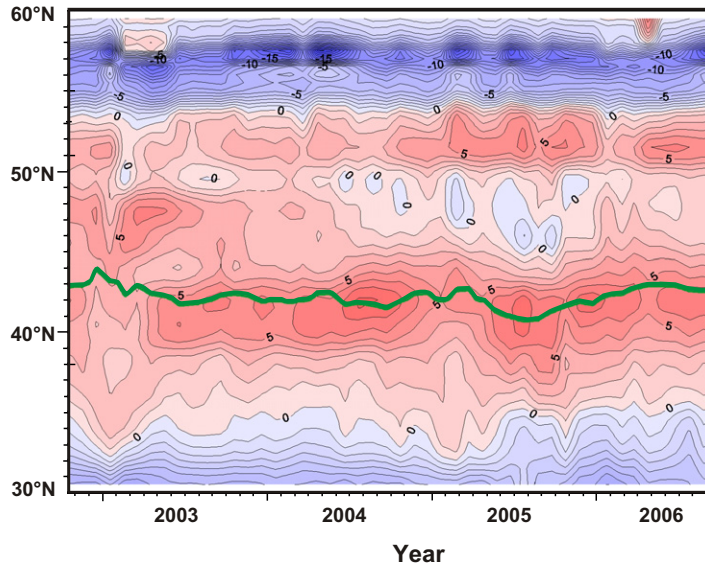


Fig. 3. Hovmöller (latitude-time) diagram of the surface zonal geostrophic current along 210°E, over the period Oct. 2002–Sept. 2006. The contour interval is 1 cm s^{-1} , with red (blue) shading for eastward (westward) directed flow. The green curve indicates the latitude of the time-dependent dividing streamline between the subpolar and subtropical gyres.

A Hovmöller diagram of the surface zonal geostrophic current from the Argo data is presented in Fig. 3. The eastward directed flow along 210°E is seen to be bound within latitudinal limits that are relatively steady in time and that coincide approximately with the latitude of the reference locations, x_{SP} and x_{ST} . On the other hand, the spatial and temporal variability within the NPC is appreciable, with the current displaying a non-uniform banded structure. The northern band of eastward directed flow is associated with a recirculation of flow in the subpolar gyre, south of the Alaskan Stream (cf. Fig. 2). The streamline separating the subpolar and subtropical gyres (shown as the green curve in Fig. 3) undergoes moderate latitudinal excursions about its mean position of 42°N at this longitude.

Fig. 4 shows time series of T'_{SP} and T'_{ST} over the 52 year period 1954–2005 from the basic numerical experiment. The first 6 years (the first two λ^{-1} periods) of the simulation, 1948–1953, were allowed for the model to adjust to the start-up of the forcing. The time series of Fig. 4 show variability on a broad range of time-scales associated with the oceanic response to time-varying wind stress curl forcing. On the other hand, the response at seasonal periods is relatively weak. This is consistent with the results of Freeland (2006) who found no evidence of a seasonal signal in 0–1000 dB dynamic height differences across the subpolar and subtropical branches of the NPC.

Overall the two time series shown in Fig. 4 are relatively weakly correlated with a coefficient of $r = 0.35$. However, it is possible to identify in these time series episodes of correlated and anti-correlated variation in the gyre transports. For example, an extended period of largely in-phase variation in T'_{SP} and T'_{ST} is found from the mid-1970s through the mid-1980s. Relatively pronounced anti-correlated variations in the transports occurred during the period 1993–2000.

To separate correlated and anti-correlated fluctuations, the time series T'_{SP} and T'_{ST} were projected onto the orthogonal modes discussed in the Appendix. The percentage of the total variance explained by the two modes in the basic experiment is given in the second column of Table 1. The dominant mode, accounting for 67% of the variance based on the reference locations ($x_{\text{SP}}, x_{\text{ST}}$), is the breathing mode identified by Freeland (2006). The bifurcation mode, in which the strength of the NPC is invariant, accounts for the remaining 33% of the total variance in the time series.

To examine the sensitivity of these results, the modal analysis was repeated using the alternative locations x_{ST}^1 , x_{ST}^2 and x_{ST}^3 to gauge the transport of the subtropical gyre. The resulting partition of variance is given in columns 3–5 of Table 1. In all cases, the breathing mode is dominant, consistent with the partition of variance

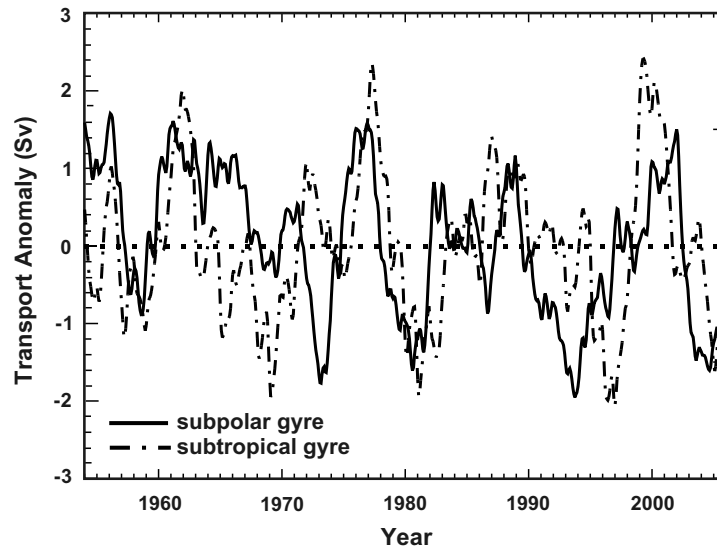


Fig. 4. Time series of model transport streamfunction at x_{SP} , representing the subpolar component of the NPC (solid line), and at x_{ST} , representing the subtropical component (dashed line).

Table 1

Fractional variance associated with the breathing and bifurcation modes of variability of the subpolar and subtropical gyres

Station pairs	(x_{SP}, x_{ST})	(x_{SP}, x_{ST}^1)	(x_{SP}, x_{ST}^2)	(x_{SP}, x_{ST}^3)
r	0.35	0.04	0.22	0.29
β^2	1.03	1.73	1.28	0.69
Breathing mode variance	67%	52%	61%	64%
Bifurcation mode variance	33%	48%	39%	36%

The results are based on time series of upper layer transport streamfunction of 52 years duration (1954–2005) from a numerical simulation. Also given is the correlation coefficient between the gyre transports, r , and the ratio of the variance of the subtropical gyre transport to that of the subpolar gyre, β^2 , as defined in the Appendix. The analysis is based on time series of gyre transport from the reference locations (x_{SP}, x_{ST}) , as well as on alternate locations for the subtropical gyre transport. These locations are defined in Section 2 and shown in Figs. 1 and 2.

found in the analysis of the Argo data. However, as the location chosen to monitor the subtropical gyre is shifted westward to a more distant location, encompassing more of the gyre transport, the dominance of the breathing mode diminishes. In the case of most westward location, x_{ST}^1 (185°E, 30°N), the two transport time series, T'_{SP} and $T'_{ST}(t) = \bar{\Psi}'(x_{ST}^1, t)$, are essentially uncorrelated ($r = 0.04$) and the breathing mode accounts for a lower fraction of the variance (52%) than the other cases.

Fig. 5 presents the amplitude coefficients of the two modes associated with the standard reference locations (x_{SP}, x_{ST}) . The time series of the breathing mode, which represents fluctuations in the intensity of the NPC, is dominated by long-period variations at decadal time-scales. Episodes of anti-correlated variability identified earlier in Fig. 4 appear as local extrema in the time series of the bifurcation mode in Fig. 5. A maximum in this mode, associated with a weakening of the subtropical gyre transport, occurs in 1982 and 1997, suggesting a connection to El Niño events.

The time series of the breathing mode in Fig. 5 indicates a major shift occurred in 1999 that may be related to events in the tropical Pacific. A strong La Niña event occurred in that year following the major El Niño of 1997/98. Fig. 5 shows a rapid shift in 1999 from negative anomalies in the NPC during 1993–1997 to strongly positive anomalies that persisted until 2002. Over 1999–2002, the average transport of the model NPC measured between x_{SP} and x_{ST} exceeds the average transport over 1993–1997 by 3.4 Sverdrups (Sv). Douglass et al. (2006) also found a significant increase in the transport of the NPC in 1999–2002 relative the earlier

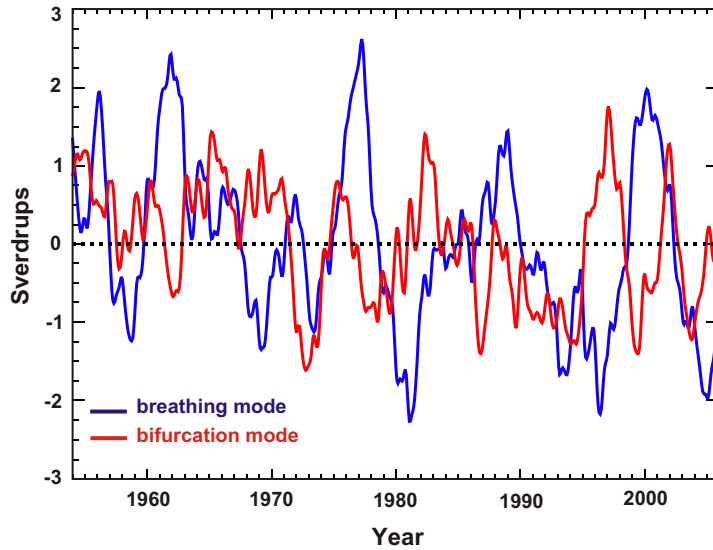


Fig. 5. Amplitude coefficients of the breathing and bifurcation modes based on reference locations ($\mathbf{x}_{SP}, \mathbf{x}_{ST}$) from the basic numerical experiment. A positive value for the breathing mode indicates a positive anomaly in the transport of the NPC. The sign of the bifurcation mode is such that a positive value for its amplitude coefficient is associated with a positive anomaly in the transport of the subpolar gyre and a compensating negative anomaly in the transport of the subtropical gyre.

period. The intensification of the NPC during the 1990s was noted previously by Qiu (2002) based on altimeter data. Fig. 5 shows the NPC weakening after 2002 with negative anomalies developing over 2003–2005. Thus with the benefit of additional years of forcing data since 2002, the results from the model suggest that there has been no long-term increase or secular trend in the transport of the NPC.

A number of additional numerical experiments were conducted to examine the sensitivity of the results to variations in model parameters. The results show a relatively weak sensitivity to variations in λ^{-1} . In particular, as λ^{-1} is varied from 5 years to 1 year, the variance of the breathing mode increases slightly from 63% to 68%. However, if the damping is omitted altogether ($\lambda = 0$), the fractional variance of this mode decreases to 56%. Reducing the value of $g'H$ from 7.5 to 6 $\text{m}^2 \text{s}^{-2}$ leaves the variance of the breathing mode essentially unchanged from the basic experiment at 68%. In summary, the results indicate that the breathing mode remains dominant in spite of significant variations in the leading parameters of the model.

3. Variability of the NPC in satellite altimeter data

In this section, SSH data from satellite altimetry are used to examine the time-varying geostrophic flow of the NPC. In particular, SSH differences across the NPC are considered and compared with numerical results and the available Argo data. For this purpose we make use of monthly SSH fields from the TOPEX/Poseidon and Jason-1 satellite altimeters, gridded at 1° resolution according to the procedure outlined in Appendix B of Lagerloef et al. (1999). Monthly means were removed from the data and the residual was smoothed twice with a 3-month boxcar filter to form SSH anomalies for the 13 year period 1993–2005.

The locations of the reference points \mathbf{x}_{SP} and \mathbf{x}_{ST} of Section 2 are indicated in Fig. 6 where they are shown with the leading empirical orthogonal function (EOF) of SSH variability over the northeast Pacific. This SSH mode, which accounts for 38% of the interannual variance, was discussed in relation to sea surface temperature variability by Cummins et al. (2005). The SSH anomaly difference, between the two points, $\Delta\eta_{NPC}(t) = \eta(\mathbf{x}_{ST}, t) - \eta(\mathbf{x}_{SP}, t)$, is taken as an index of the surface geostrophic transport associated with fluctuations of the NPC. The mode of SSH variability shown in Fig. 6 suggests a major transition in late 1998 from negative to positive anomalies of $\Delta\eta_{NPC}$, leading to an intensification of the NPC that lasted until late 2002. The principal component associated with this mode (PC1) subsequently relaxes to small negative values

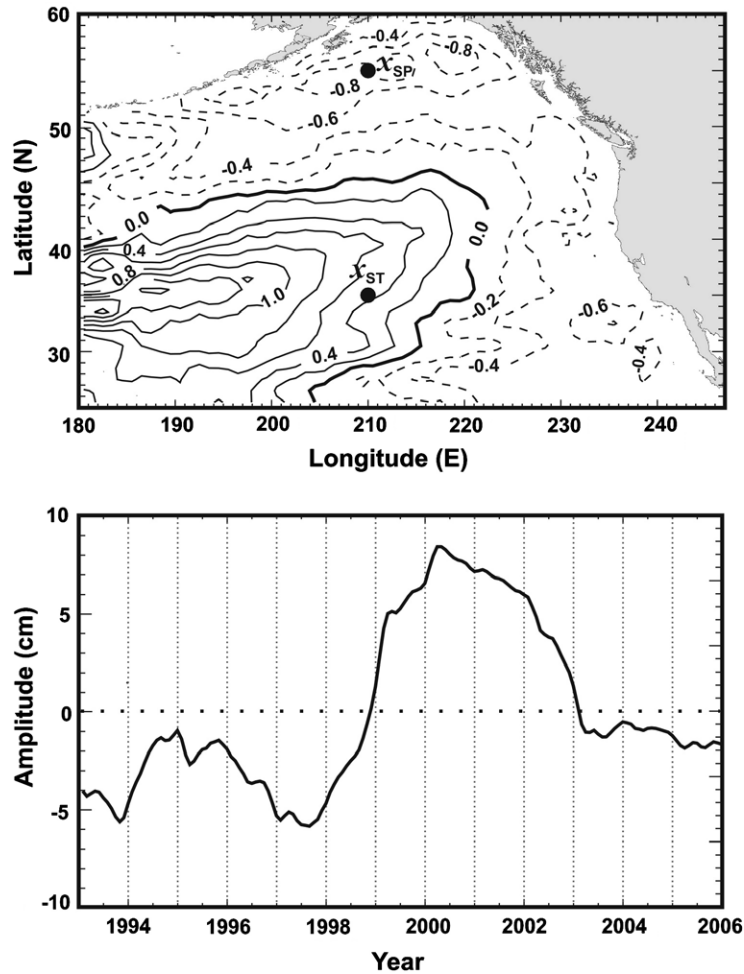


Fig. 6. Leading EOF (top panel) and principal component (lower panel) of sea surface height over the northeast Pacific. Also included are the reference locations, x_{SP} and x_{ST} , that are used to form an index of the surface geostrophic transport of the NPC. The EOF spatial pattern has been normalized to have a minimum value of -1 and is contoured at intervals of 0.2 .

to the end of the record. While higher modes also contribute to the total variability of $\Delta\eta_{NPC}$, given that the leading mode accounts for a considerable fraction of the interannual variance and that the major change in SSH that occurred in 1998/99 projects very strongly onto this mode (Cummins et al., 2005), it may be expected that variability of $\Delta\eta_{NPC}$ will be markedly influenced by this leading EOF.

The bipolar spatial pattern of the EOF of Fig. 6 is dominated by SSH variability of opposite sign between the subtropical and subpolar (Gulf of Alaska) regions. As such, this spatial pattern represents a breathing mode and is associated with in-phase variations in the transport of the subtropical and subpolar gyres. For example, the mode indicates that the SSH difference between point x_{ST} and the coast along $35^\circ N$ is positive ($\partial\eta/\partial x > 0$) over the period 1993–1998, indicating anomalously weak transport in the subtropical gyre (California Current). There is a reversal in the sign of this gradient in 1999–2002, during which time the subtropical gyre transport is enhanced. Likewise, point x_{SP} is located in a local minimum in the EOF pattern of Fig. 6. Thus, for this mode of variability, the gradient between x_{SP} and the eastern boundary is anomalously negative ($\partial\eta/\partial x < 0$) during 1993–1998, and positive during 1999–2002, reflecting the concomitant strengthening of the transport of the subpolar gyre (Alaska Current) between these two periods. Finally, a notable aspect of the EOF is that the spatial pattern is of constant sign along the coastal boundary from Baja California to the Aleutian Islands. Thus the mode represents in-phase SSH variations along the length of the coast, consistent with the results of Chelton and Davis (1982).

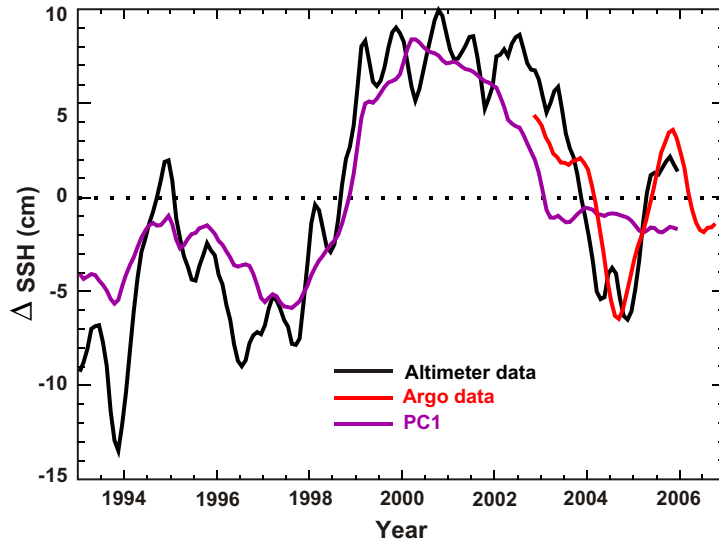


Fig. 7. The black curve is an index of the variability of the surface geostrophic transport of the NPC based on SSH differences between the reference locations x_{SP} and x_{ST} . For comparison, the curve shown in purple is the principal component of the SSH mode presented in Fig. 6. The red curve shows smoothed anomalies of dynamic height difference across the NPC based on observations from Argo.

Notwithstanding the co-variability of the gyre transports evident in the leading mode of Fig. 6, no attempt is made to establish separate indices for the transport of the subpolar and subtropical components of the NPC with the altimeter data. This would require defining an additional reference location situated along the time-varying streamline separating the gyres. While such a dividing streamline can be identified readily in the geostrophic circulation fields derived from the Argo data, this is not the case for the altimeter data which provide only SSH anomalies. This limitation should be overcome eventually with the development of precise information regarding the earth's geoid.

The variation of $\Delta\eta_{NPC}(t)$ over the 13-year period, 1993–2005, is presented in Fig. 7. For comparison, the figure also includes PC1, the principal component of the EOF of Fig. 6, as well as the dynamic height difference across the NPC derived from the Argo data over the 4-year period Oct. 2002–Sept. 2006. The dominant signal seen in the altimeter data is a low frequency variation in the intensity of the NPC, which reaches its maximum during 1999–2002. This signal is very well described by the principal component of the leading SSH mode. However, after 2002, the amplitude coefficient of this mode is relatively small, and it ceases to reflect fluctuations in the strength of the NPC. Thus additional EOFs are required to describe variations in the NPC after 2002. Fig. 7 also indicates that the variation in dynamic height across the NPC from the Argo observations is in good agreement with the altimeter-based SSH index. This shows the NPC reaching a minimum in 2004 and subsequently intensifying to reach a new maximum in late 2005. The Argo data then indicate a relaxation of the NPC in 2006.

The indices of NPC variability based on SSH differences between reference points x_{SP} and x_{ST} and between x_{SP} and x_{ST}^2 are presented in Fig. 8a and b, respectively. These time series (shown as black curves) have been normalized by their respective standard deviations. For comparison, Fig. 8a and b include the normalized transport streamfunction anomaly from the quasi-geostrophic model for the period 1993–2005 (the purple curves). This comparison shows that there is a rather close correspondence between the index of the NPC derived from the altimeter data and the model transport streamfunction; the correlation coefficient between the two is $r = 0.80$ and $r = 0.84$ in Fig. 8a and b, respectively. In particular, the model captures the major signal of the record, which is the transition to a strengthened NPC during the period 1999–2002. The relaxation of this event in late 2002–2003 is also seen in the model results, albeit with some differences in timing in Fig. 8a. Overall, the correspondence between model and data in Fig. 8 suggests that the major variability of the NPC over the period of the altimeter observations was driven by anomalous wind stress curl forcing.

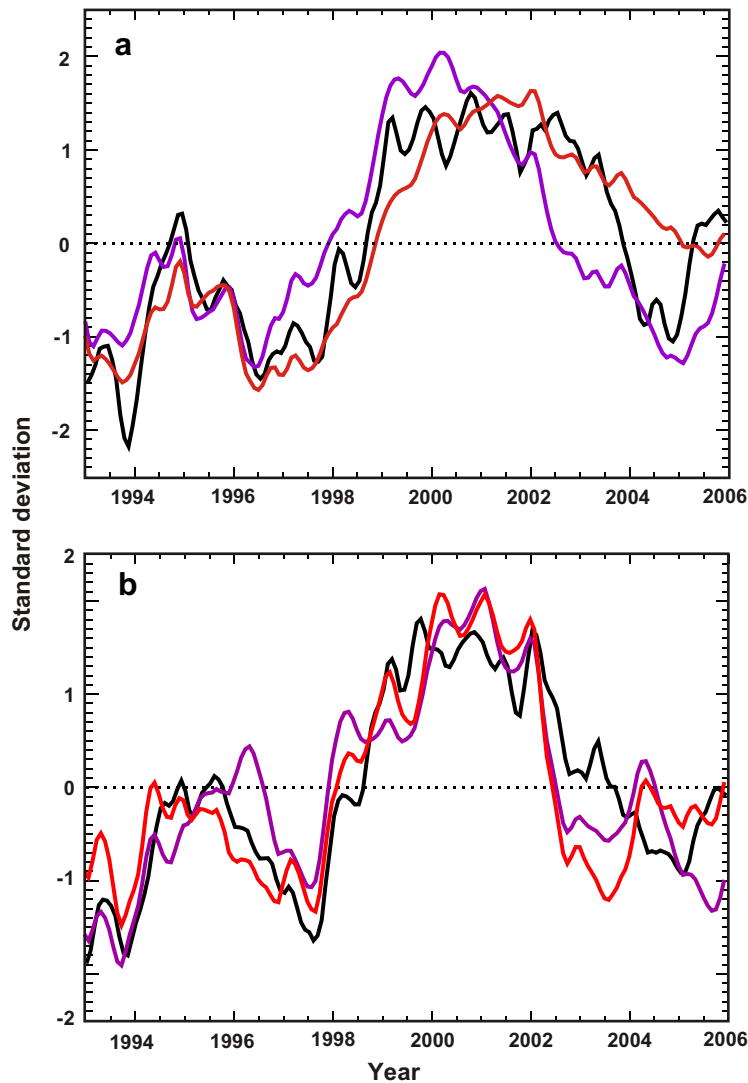


Fig. 8. (a) Comparison between time series of anomalies of SSH difference across the NPC (black curve) and the model transport anomalies (purple curve) based on the reference points x_{SP} and x_{ST} . The red curve is from an additional numerical experiment in which the beta effect was suppressed. All time series have been normalized by their respective standard deviations. (b) As in (a), except based on reference locations x_{SP} and x_{ST}^2 (195°E, 32°N).

3.1. Discussion

The strong correlation between time series of fluctuations of the NPC from altimeter data and the model streamfunction (Fig. 8) indicates that anomalous wind forcing is likely the dominant factor driving the observed low frequency ocean variability. Douglass et al. (2006) also suggested that wind forcing plays an important role in this regard. In particular, they hypothesized that the intensification of the NPC during the period 1999–2002, relative to the period 1992–1995, is associated with changes in the Sverdrup-balanced transport.

To address this matter, an additional numerical experiment was conducted with the quasi-geostrophic model. In this case, the advection of planetary vorticity (the beta effect) was suppressed, thus eliminating Rossby waves and Sverdrup-balanced flow from the simulation. Variations in the transport of the NPC from this simulation are shown as the red curves in Fig. 8a and b. The low frequency variation of the NPC in this exper-

iment is similar to that of the basic case, and the time series are just as well correlated with the altimeter data ($r = 0.85$ and $r = 0.89$ for Fig. 8a and b, respectively) as the cases in which the beta effect has been included.

This agreement suggests that neither changes in Sverdrup-balanced transport nor Rossby wave propagation are essential to model the dominant low frequency variability of the NPC during the period in question. Rather, these results provide further support for the view that variability of upper ocean currents at large scales over the northeast Pacific occurs in response to differential Ekman pumping (Reed, 1984). To represent variability on interannual to decadal time-scales, it is necessary to include a damping term (Lagerloef, 1995), yielding a model that has the form of a stochastic climate model. Such models have demonstrated skill in representing low frequency variability in upper layer thickness seen in observations (Cummins and Lagerloef, 2002) and in ocean general circulation models of the northeast Pacific (Capotondi et al., 2005). In addition, Cummins and Lagerloef (2004) have shown that a stochastic climate model driven by Ekman pumping can account for the leading mode of SSH variability over this region (Fig. 6). It is due, in part, to the ability to represent this mode that the model is able to account for the fluctuations of the NPC demonstrated in Fig. 8.

4. Summary

This study has considered the geostrophic flow of the NPC and the modes of variability of its subpolar and subtropical components. In particular, dynamics heights from Argo, numerical simulations and satellite altimeter data were used to examine and quantify the relative strength of two orthogonal modes of variability, termed the breathing and bifurcation modes by Freeland (2006). The former involves in-phase fluctuations in the transport of the subpolar and subtropical gyres associated with changes in the strength of the NPC. Conversely, for the bifurcation mode, discussed originally by Chelton and Davis (1982), the strength of the NPC is invariant, and fluctuations in the transport of the subpolar and subtropical gyres are anti-correlated.

Time series from numerical simulations of wind-driven variability extending for over 50 years duration show the occurrence of episodes of both correlated and anti-correlated variation in the transport of the subpolar and subtropical gyres. A decomposition of these time series shows that typically two-thirds of the variance resides in the breathing mode. These results are in good agreement with a similar analysis of the relatively short-time series of dynamic heights from the Argo data. Thus the dominance of the breathing mode is consistent with the statistical properties of a linear ocean model in which the variability is directly driven by wind forcing.

Over the period of the altimeter data, the low frequency variability of the NPC was shown to be associated with the leading EOF of SSH over the northeast Pacific. The spatial structure of this regional mode reflects in-phase fluctuations in the transport of the subpolar and subtropical gyres, consistent with analyses of the Argo data and numerical simulations which find the breathing mode to be dominant.

A strong correlation is found between SSH differences across the NPC and variations in the transport streamfunction of the numerical simulation. This agreement provides compelling evidence that fluctuations in the strength of the NPC are driven by changes in wind forcing. This strong correlation is maintained in an additional numerical simulation in which the beta effect was suppressed, suggesting that variability of the NPC is associated with large-scale differential Ekman pumping rather than Rossby wave propagation or changes in the Sverdrup-balanced transport. This is consistent with the results of Lagerloef (1995) and Cummins and Lagerloef (2004) and provides further evidence that a stochastic climate model driven by Ekman pumping can account for SSH variability at large scales over the northeast Pacific.

Acknowledgements

This work was presented, in part, at the PICES/DFO Symposium on “Time Series of the N.E. Pacific: A Symposium to mark the 50th anniversary of Line P” in Victoria, BC, Canada, July 2006. We are grateful to Fisheries and Oceans Canada and PICES for their sponsorship of the meeting. The gridded altimeter data were obtained from Prof. Gary Mitchum of the University of South Florida. The Argo data were collected and made available by the International Argo Project and national programs that contribute to it. Argo is a pilot program of the Global Ocean Observing System. We are grateful to the referees for the careful attention they have given to the paper.

Appendix. Decomposition into breathing and bifurcation modes

Given time series of zero mean, $T_1(t)$ and $T_2(t)$, representing the geostrophic transport anomalies of two gyres, we consider a decomposition of these time series into orthogonal components, termed breathing and bifurcation modes, whose amplitude coefficients are denoted by $a(t)$ and $b(t)$, respectively. Fluctuations in $b(t)$ represent mutually compensating variations of the transport into each gyre, while the total transport, $T_1(t) + T_2(t)$, is invariant. Conversely, fluctuations in $a(t)$ are proportional to variations in the total transport.

A suitable transformation between (T_1, T_2) and (a, b) is given by

$$\begin{pmatrix} T_1 \\ T_2 \end{pmatrix} = \begin{bmatrix} \frac{1}{\sqrt{2}} & \frac{1}{\sqrt{2}} \\ \frac{1}{\sqrt{2}} & -\frac{1}{\sqrt{2}} \end{bmatrix} \begin{pmatrix} a \\ b \end{pmatrix}.$$

The columns of this matrix are orthogonal unit vectors that conserve the total variance, $\sigma^2 = \langle T_1^2 \rangle + \langle T_2^2 \rangle = \langle a^2 \rangle + \langle b^2 \rangle$, with the angle brackets denoting a time average. It may be noted that generally $\langle ab \rangle \neq 0$, and that there is a non-zero correlation between $a(t)$ and $b(t)$. Thus, the amplitude coefficients are distinct from the principal components of $T_1(t)$ and $T_2(t)$.

The fraction of variance in the breathing and bifurcation modes is given by $R_1 = \langle a^2 \rangle / \sigma^2$ and $R_2 = \langle b^2 \rangle / \sigma^2$, respectively. Since $\langle a^2 \rangle = \frac{1}{2} \langle (T_1 + T_2)^2 \rangle$ and $\langle b^2 \rangle = \frac{1}{2} (\langle T_1^2 \rangle + \langle T_2^2 \rangle - 2\langle T_1 T_2 \rangle)$, it is possible to express the modal variances as

$$(R_1, R_2) = \left(\frac{1}{2} + \frac{r\beta}{1 + \beta^2}, \frac{1}{2} - \frac{r\beta}{1 + \beta^2} \right),$$

where $r = \langle T_1 T_2 \rangle / \langle T_1^2 \rangle^{1/2} \langle T_2^2 \rangle^{1/2}$ is the correlation coefficient between T_1 and T_2 , and β^2 is the ratio of the variance of the transports, e.g., $\beta^2 = \langle T_1^2 \rangle / \langle T_2^2 \rangle$. Hence, when the transport anomalies of the gyres are positively (negatively) correlated, the breathing (bifurcation) mode is dominant. If the gyres are uncorrelated ($r = 0$), then the variance is partitioned equally between the modes.

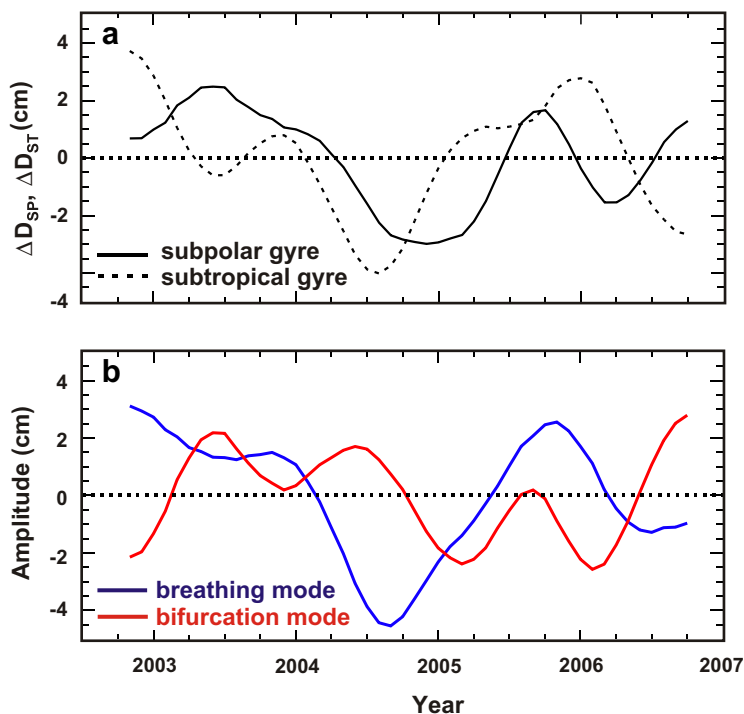


Fig. A1. (a) Smoothed time series of dynamic height differences across the subpolar and subtropical gyres from Argo. (b) Time series of the amplitude coefficients associated with the breathing and bifurcation modes.

Following Freeland (2006), 0–1000 dB dynamic height differences across the subpolar and subtropical gyres in the northeast Pacific are taken as a proxy for the geostrophic transport. These dynamic height differences are obtained from monthly gridded fields that were constructed from the Argo float observations by projecting the data onto the first 20 EOFs of the reduced-gravity model (Freeland and Cummins, 2005). Such a projection yields smooth fields that account typically for 85–90% of the spatial variance of the monthly observations.

The top panel in Fig. A1 presents time series of smoothed dynamic height differences across the subtropical and subpolar gyres from the Argo data for the 4-year period, Oct. 2002–Sept., 2006. A 5-month boxcar filter was applied twice to suppress the short time-scale noise present in the raw time series. Decomposition of the smoothed time series according to the procedure described above yields 65% of the variance in the breathing mode and 35% in the bifurcation mode. The correlation coefficient between the gyres is $r = 0.31$ and the ratio of the variance of the subtropical gyre to that of the subpolar gyre is $\beta^2 = 1.4$. It may be expected that the progressive addition of uncorrelated noise to T_1 and T_2 will lead to an equipartition of variance between the two modes. Accordingly, shortening the window of the boxcar filter to 3 months reduces the variance of the breathing mode to 60%. If the smoothing is omitted altogether, it is further reduced to 52%.

The lower panel of Fig. A1 presents the modal amplitudes $a(t)$ and $b(t)$. It is evident that these time series are dominated by low frequency variability, particularly in the case of the breathing mode. Thus the time series are relatively short compared to the dominant time-scales and it is likely that a longer record is necessary to establish a stable estimates of the partition of variance between the two modes.

References

- Capotondi, A., Alexander, M.A., Deser, C., Miller, A.J., 2005. Low-frequency pycnocline variability in the northeast Pacific. *Journal of Physical Oceanography* 35, 1403–1420.
- Chelton, D.B., Davis, R.E., 1982. Monthly mean sea-level variability along the west coast of North America. *Journal of Physical Oceanography* 12, 757–784.
- Cummins, P.F., Lagerloef, G.S.E., 2002. Low-frequency pycnocline depth variability at Ocean Weather Station P in the northeast Pacific. *Journal of Physical Oceanography* 32, 3207–3215.
- Cummins, P.F., Lagerloef, G.S.E., 2004. Wind-driven interannual variability over the northeast Pacific Ocean. *Deep-Sea Research I* 51, 2105–2121.
- Cummins, P.F., Lagerloef, G.S.E., Mitchum, G., 2005. A regional index of northeast Pacific variability based on satellite altimeter data. *Geophysical Research Letters* 32, L17607. doi:10.1029/2005GL023642.
- Douglass, E., Roemmich, D., Stammer, D., 2006. Interannual variability in northeast Pacific circulation. *Journal of Geophysical Research* 111, C04001. doi:10.1029/2005JC003015.
- Freeland, H.J., 2006. What proportion of the North Pacific Current finds its way into the Gulf of Alaska? *Atmosphere-Ocean* 44, 321–330.
- Freeland, H.J., Cummins, P.F., 2005. Argo: a new tool for environmental monitoring and assessment of the world's oceans, an example from the N.E. Pacific. *Progress in Oceanography* 64, 31–44.
- Fu, L.-L., Qiu, B., 2002. Low frequency variability of the North Pacific Ocean: the roles of boundary- and wind-driven baroclinic Rossby waves. *Journal of Geophysical Research* 107, 3220. doi:10.1029/2001JC001131.
- Kalnay, E., Kanamitsu, M., Kistler, R., Collins, W., Deaven, D., Gandin, L., Iredell, M., Saha, S., White, G., Woollen, J., Zhu, Y., Chelliah, M., Ebisuzaki, W., Higgins, W., Janowiak, J., Mo, K.C., Ropelewski, C., Wang, J., Leetmaa, A., Reynolds, R., Jenne, R., Joseph, D., 1996. The NCEP/NCAR 40 reanalysis project. *Bulletin of the American Meteorological Society* 77, 437–471.
- Lagerloef, G.S.E., 1995. Interdecadal variations in the Alaska gyre. *Journal of Physical Oceanography* 25, 2242–2258.
- Lagerloef, G.S.E., Mitchum, G.T., Lucas, R.B., Niiler, P.P., 1999. Tropical Pacific near-surface currents estimated from altimeter wind and drifter data. *Journal of Geophysical Research* 104, 23313–23326.
- Qiu, B., 2002. Large-scale variability in the midlatitude subtropical and subpolar North Pacific Ocean: observations and causes. *Journal of Physical Oceanography* 32, 353–375.
- Reed, R.K., 1984. Flow of the Alaskan Stream and its variations. *Deep-Sea Research* 31, 369–386.
- Zhang, Y., Wallace, J.M., Battisti, D.S., 1997. ENSO-like interdecadal variability: 1900–93. *Journal of Climate* 10, 1004–1020.